Single photoionization of the Zn II ion in the photon energy range 17.5 to 90.0 eV: experiment and theory

G. Hinojosa[1]⋆, V. T. Davis[2], A. M. Covington[2], J. S. Thompson[2],
A. L. D. Kilcoyne[3], A. Antillón[1], E. M. Hernández[1,7], D. Calabrese[4],
A. Morales-Mori[1], A. M. Juárez[1], O. Windelius[5,6] and B. M. McLaughlin[8,9]†

[1]*Universidad Nacional Autónoma de México, Instituto de Ciencias Físicas, AP 48-3, Cuernavaca 62251, México*
[2]*Department of Physics, University of Nevada, Reno, NV 89557-0220, USA*
[3]*The Advanced Light Source, Lawrence Berkeley National Laboratory, Berkeley, California 94720, USA*
[4]*Department of Physics, Sierra College, Rocklin, CA 95677, USA*
[5]*Department of Applied Physics, Chalmers University of Technology, S-41296 Göteborg, Sweden*
[6]*Department of Physics, University of Gothenburg, SE-412 96, Göteborg, Sweden*
[7]*Universidad Autónoma del Estado de Morelos, Avenida Universidad 1001, Cuernavaca 62209, México*
[8]*Centre for Theoretical Atomic and Molecular Physics (CTAMOP), School of Mathematics and Physics,*
Queen's University Belfast, Belfast BT7 1NN, UK
[9]*Institute for Theoretical Atomic and Molecular Physics (ITAMP)*
Harvard Smithsonian Center for Astrophysics, MS-14, Cambridge, MA 02138, USA

ABSTRACT
Measurements of the single photoionization cross section of Cu-like Zn^+ ions are reported in the energy (wavelength) range 17.5 eV (709 Å) to 90 eV (138 Å). The measurements on this *trans*-Fe element were performed at the Advanced Light Source synchrotron radiation facility in Berkeley, California at a photon energy resolution of 17 meV using the photon-ion merged-beams end-station. Below 30 eV the spectrum is dominated by excitation autoionizing resonance states. The experimental results are compared with large-scale photoionization cross-section calculations performed using a Dirac Coulomb R-matrix approximation. Comparison are made with previous experimental studies, resonance states are identified and contributions from metastable states of Zn^+ determined.

Key words: atomic data – atomic processes – scattering

1 INTRODUCTION

About half of the heavy elements (Z ≥30) in the Universe were formed during the Asymptotic Giant Branch (AGB) phase through slow neutron-capture (*n*-capture) nucleosynthesis (the *s*-process). In the intershell between the H- and He-burning shells, Fe-peak nuclei experience neutron captures interlaced with β-decays, which transform them into heavier elements. For example, in spite of its cosmic rarity, atomic selenium has been detected in the spectra of stars (Roederer 2012; Roederer et al. 2014) and of astrophysical nebulae (Sterling & Dinerstein 2008; Sterling et al. 2009; García-Rojas et al. 2015; García-Rojas et al. 2016). The chemical composition of these objects illuminate de-

tails of stellar nucleosynthesis and the chemical evolution of galaxies. To interpret such astrophysical spectra requires three types of fundamental parameters: i) the energy of internal states (or transition frequencies), ii) transition probabilities (or Einstein A-coefficients), and iii) collisional excitation rate coefficients (or collision strengths in the case of electron impact). While these parameters have been studied over the past century for many atomic and molecular species, the necessary information is far from complete or is of insufficient reliability. Extensive databases do exist for the first two items (e.g., NIST), referred to as spectroscopic data; the situation for the last item is far less satisfactory.

However, atomic data, such as PI cross sections, are unknown for the vast majority of *trans*-Fe, neutron-capture element ions. We note that the *n*-capture elements, Cd, Ge, and Rb, were recently detected in planetary nebulae (Sterling et al. 2016). Measurements for the photoionization cross

⋆ E-mail:hinojosa@icf.unam.mx
† E-mail:bmclaughlin899@btinternet.com

section on the *trans-Fe* element Se, in various ionized stages (Sterling et al. 2011a,b; Sterling & Witthoeft 2011; Esteves et al. 2011, 2012; Macaluso et al. 2015) provided critically needed data to astrophysical modelers (Sterling & Stancil 2011; Sterling et al. 2015; García-Rojas et al. 2016), and was benchmarked against results from a recently developed suite of fully relativistic parallel Dirac Atomic R-matrix (DARC) codes (Ballance 2016; McLaughlin & Ballance 2012a,b, 2015; McLaughlin et al. 2016, 2017) with excellent agreement being achieved.

Studies of Zn I abundance in metal-poor stars are used to infer the histories of galactic chemical evolution. Unfortunately, a major source of uncertainty in all these studies is a lack of accurate knowledge of atomic parameters, such as transition wavelengths, cross sections for photoionization (PI), electron-impact excitation (EIE), dielectronic recombination (DR), and line-strengths (Sneden et al. 1991; Mishenina et al. 2002; Roederer et al. 2011, 2010; Frebel et al. 2014).

Photoionization of atomic ions is an important process in determining the ionization balance and the abundances of elements in photoionized astrophysical nebulae. It has recently become possible to detect neutron n-capture elements (Se, Cd, Ga, Ge, Rb, Kr, Br, Xe, Ba and Pb) in a large number of ionized nebulae (Sterling et al. 2007; Sharpee et al. 2007; Sterling & Dinerstein 2008). These elements are produced by slow or rapid n-capture nucleosynthesis. Measuring the abundances of these elements helps to reveal their dominant production sites in the Universe, as well as details of stellar structure, mixing and nucleosynthesis (Sharpee et al. 2007; Langanke & Wiescher 2001; Sterling et al. 2016). These astrophysical observations are the motivation to determine the EIE, EII, PI, and recombination properties of n-capture elements (Cardelli et al. 1993; Smith & Lambert 2015; Wallerstein et al. 1997; Busso et al. 1999; Langanke & Wiescher 2001; Travaglio et al. 2004; Herwig 2005; Cowan & Sneden 2006).

The validity of various theories of galactic evolution, stellar nucleosynthesis, the interplay of gravity and chemistry in various stellar bodies all depend on accurate measurements of metals within different types of astrophysical objects such as large stars, nebulae and globular clusters (Sneden et al. 1991; Chayer et al. 2005; Mishenina et al. 2002; Roederer et al. 2011; Jose & Iliadis 2011; Hinkel et al. 2014; Nissen et al. 2007, 2004; Chen et al. 2004; Hollek et al. 2011; Kobayashi & Nomoto 2009; Djeniže, S. et al. 2003). The oldest parts of the Milky Way galaxy are the metal-poor stars in the thick disk. The origin and evolution of the chemical and dynamical structures of the thick disk remain unclear. Chemical abundances in stars of the thick disk, and in the inner and outer halo stars are important because the ratios of heavy elements to Fe in these stars can reveal different formation mechanisms. [Zn/Fe] ratios in outer halo stars can be used to distinguish formation timescales of these stars from those of stars in the disk (Nissen et al. 2004; Chen et al. 2004; Tumlinson 2006).

The relevance that atomic parameters have in astrophysics and in our understanding of the chemical evolution and the chemical assembly of progenitor nebulae is derived from measurements of elemental abundances of zinc. In these nebulae, zinc happens to be a better indicator of Fe and Fe-group abundances, as it does not condense into dust as

easily as iron. Some nebulae do not show the abundance of Zn that models predict, indicating that reliable data on this species are of critical importance in the study of these systems (Karakas et al. 2009).

Experimental studies on the photoionization (PI) of ions from intermediate-sized atoms provide a wealth of spectroscopic data and cross section values. PI cross section data on *trans*-Fe ions can be used to advance theoretical models in light of details that substantial photon flux and high energy resolution have the power to reveal. To our knowledge, the only data available on the PI of the *trans*-Fe element, Zn II, is the pioneering experimental work by Peart et al. (1987), using a merged-beams technique by combining synchrotron radiation (SR) with a beam of Zn^+ at the Daresbury radiation facility. Peart et al. (1987) succeeded in observing several resonances and measured the photoionization cross section with moderate photon energy resolution, at the Daresbury beam line (Lyon et al. 1986, 1987; Peart et al. 1987), which had an energy resolution ($\Delta\lambda$) ranging from 0.2 – 1 Å, or approximately 20 meV – 4 meV (Lyon et al. 1986). Since the photon flux for measurements on Zn II ions (Peart et al. 1987) was low, a direct measurement of the background photoionization cross section was not possible nor was identification of the peaks in the spectrum. The previous work of Peart et al. (1987) however may be used for comparison purposes and verification of the data presented here.

Previous studies on the PI of Zn I and species iso-electronic to Zn II, relevant to the present work have been performed by Harrison et al. (1969), who studied PI of the neutral Zn atom, using UV discharge sources. Müller et al. (1986) studied PI of the iso-electronic neutral Cu atom. From a theoretical point of view, Zn I is the first transition metal with a closed d-shell with possible np resonances (Stener & Decleva 1997). Apart from its fundamental importance, in astrophysics, photoionization of Zn^+ (Zn II) is of great practical interest. Recently, Ganeev et al. (2016) demonstrated that autoionizing states of Zn II and Zn III have the ability to enhance harmonics in laser-produced plasmas. We note the K_α X-ray spectrum of the Cu atom has also been measured recently by Mendenhall et al. (2017). Autoionizing states are, in general, excited states with energies that are not commonly studied in the literature. In the present work, energies for several of these intermediate autoionizing resonant states have been measured and identified.

The prime motivation for the present study of this *trans*-Fe element, Zn II, is to provide benchmark PI cross section data for applications in astrophysics. High-resolution measurements of the photoionization cross section of Zn^+ were performed at the ALS synchrotron radiation facility in Berkeley, California, over the photon energy range 17.4 – 90 eV at a resolution of 17 meV FWHM. Several highly excited states have been identified in the energy (wavelength) range 20 eV (620 Å) to 90 eV (138 Å). The high resolution ALS photoionization cross sections are used to benchmark large-scale DARC calculations in this same energy interval. A comparison of the DARC PI cross sections with previous experimental studies (Peart et al. 1987) and the present ALS work indicate excellent agreement, providing further confidence in the data for various astrophysical applications.

2 EXPERIMENT

The present experimental technique and apparatus have been described in detail previously by Covington et al. (2002). Recent improvements to the technique have been discussed by Müller and collaborators (Müller et al. 2014; Müller et al. 2015). Here, we present a brief description with details relevant to the present measurements. The experimental method is known as the merged-beams technique (Peart et al. 1973; Lyon et al. 1986, 1987). The method consists of overlapping trajectories of two beams; in this case, a photon beam from the Advanced Light Source (ALS) synchrotron at the Lawrence Berkeley National Laboratory and a counter-propagating ion beam of Zn^+ ions. The experiment was designed to count the resulting Zn^{2+} ions and measure the relevant parameters of the ion and photon beams as well as their spatial overlap.

The photon beam was generated by a 10-cm-period undulator located in the synchrotron ring. The synchrotron was operated under an almost constant electron current of 0.5 A at 1.9 GeV. The resulting photon beam had a maximum width of 1.5 mm and a divergence less than 0.06^o. In the grazing incidence mode, the photon beam was directed onto a spherical grating with controls that allowed changes to the photon beam energy to be made as desired.

We used a side-branch gas cell with either He or Kr gases to calibrate the photon energy in the energy range from 18.601 eV to 92.437 eV (Domke et al. 1996; King et al. 1977). A polynomial fit to reference energy values was used to calibrate the energy scale (along with the Doppler shift correction due to the counter-propagating photon and ion beams). As a result of the calibration, our data is in agreement with the values reported by NIST (Kramida et al. 2016) to 3 significant figures. The uncertainty associated with this procedure is estimated to be ± 10 meV. The Zn^+ ion beam was produced with an all-permanent magnet ECR ion source by evaporating zinc in an oven that was inserted into the ion source chamber, with argon used as a support or buffer gas. A 60° - sector analyzing magnet was used to separate (as a function of its momentum-to-charge ratio) the Zn^+ cations which had a kinetic energy of 6 keV. A cylindrical Einzel lens, two sets of steering plates, and a set of slits were used to focus and collimate the ion beam. A set of electrostatic 90° spherical-sector plates was used to merge the ion beam with the photon beam.

The ions then entered a voltage-biased cylindrical interaction region (IR), Zn^{2+} photo-ions produced inside it had a different energy as compared to those produced outside, thereby energy-labeling the ions generated within the specific length of the IR. Energy-tagged Zn^{2+} ions were subsequently separated from the primary Zn^+ ion beam by a 45° dipole analyzing magnet. The experiment was carried out in two different operational modes. The purpose of the first operational mode was to obtain precise knowledge of the interaction length and beam overlap in order to measure the cross section. In this operational mode, the overlap of the two beams within the IR was carefully measured at discrete photon energies.

An absolute-calibrated photo diode was used while operating in this mode. In the second mode, the photo-ion signal was maximized without monitoring the actual overlap of the beams within the IR. While running in this mode,

Table 1. Zn^+ absolute single-photoionization valence shell cross section made at the ALS with a 17 ± 3 meV photon energy resolution in the photon energy range 25 - 90 eV.

Energy (eV)	σ (Mb)
25.0	1.14 ± 0.23
29.8	7.83 ± 1.60
35.0	9.80 ± 1.80
45.0	9.99 ± 2.00
60.0	11.20 ± 2.24
78.0	9.73 ± 1.95
89.5	10.60 ± 2.14

the IR voltage was also maintained at all times and the beams overlap was monitored at only some photon energies between successive energy range scans, resulting in a photo-ion yield spectrum that was later normalized to the absolute measurements. The purpose of measuring spectroscopic energy-scans with the IR voltage on was to measure the absolute cross sections by slightly tuning back the overlap at the pre-established photon energies. Integration times of 200s were used to account for the stabilization time of the photo-diode current reading.

The Zn^+ ion beam was measured by an extended Faraday cup. The resulting Zn^{2+} photo-ions were counted of the dipole analyzing magnet whose magnetic field was adjusted so that only product photo-ions generated inside the interaction region were collected. In addition, by using a chopper wheel in the photon beam, the Zn^{2+} signal was background-subtracted to remove those ions that were produced by collisions with residual gas in the IR. To derive absolute PI cross sections, two-dimensional beam profiles of the ion beam $I^+(x, y)$ and the photon beam $I(x, y)$ were measured and used to calculate the interaction volume of the two beams. Three beam translating-slit profilers were used to sample the form factor $F(z)$ according to

$$F(z) = \frac{\int \int I^+(x, y) I^\gamma(x, y) dx dy}{\int I^+(x, y) dx dy \int I^\gamma(x, y) dx dy} \qquad (1)$$

where z is the reference axis assigned to the propagation direction of the ion beam. $F(z)$ was measured at three positions, at the entrance, in the centre and at the exit of the IR. Measured values of these positions were labeled as $i =1$, 2, 3, respectively. With these three values of $F_i(z)$, $F(z)$ was interpolated within the IR length and integrated over z to compute the spatial overlap of the photon and ion beams along the common IR path.

Absolute cross section measurements were performed at specific photon energies (open circles (magenta) in Fig.1 (a) and (b)) where no resonant structure was present in the spectrum and are tabulated in Table 1. The single-photoionization cross section for Zn^+ was derived from the expression

$$\sigma = \frac{Rqe^2 \nu_i \epsilon}{I^+ I^\gamma \int F(z) dz}, \qquad (2)$$

where R is the photo-ion count rate, $q=1$ is the charge state of Zn^+, $e=1.6 \times 10^{-19}$ C, ν_i is the ion beam velocity in cm/s, ϵ is the responsivity of the photo-diode (electrons per photon), I^+ is the ion beam current (A), and I^γ is the photo-

Table 2. The correction factor f_c applied to the present measured ALS cross section data due to the presence of high-order radiation effects in the photon beam. In our work, we interpolated the values from Müller et al. (2015) and included values at 30 eV and 35 eV.

Photon energy (eV)	Correction factor f_c
16	1.90^a
20	1.40^a
25	1.17^a
30	1.07^b
35	1.00^b

[a]Values determined by Müller et al. (2015).
[b]Present values.

diode current (A). In this experiment, the photo-ion counting efficiency was practically 100%.

The largest sources of systematic error originate from the beam-overlap integral, the beam profile measurements, and the photo-diode responsivity function. Other contributions to the total systematic error are listed in Covington et al. (2002). All sources of systematic error combine to yield a total uncertainty of 20%, estimated at the 90% confidence level.

The spectra shown in Fig.1 and in panel (a) of Fig. 2 were measured at 5 to 10 eV-wide photon energy intervals. Each interval overlapped its neighbouring intervals by 1.0 eV. All the individual parts of the spectra were later combined by joining adjacent regions to produce the entire measured spectrum. An estimation of the photon energy uncertainty caused by this gluing procedure was not greater than ±8 meV.

The overall energy uncertainty propagated by both the gas cell energy calibration and the data reduction procedure is ±13 meV. The photo-ion yield spectra were normalized by using the measurements at the discrete photon energies of the absolute photoionization cross section.

It is important to point out that corrections in the cross section caused by higher-order radiation in the photon beam (mainly second- and third-order radiation in the lower energy regime) can be significant in this photon beam line. The correction to the cross section at 20 eV was estimated to be almost 40% by Müller et al. (2015) who derived a correction function f_c for this photon beam-line. The error of this correction is 50% of the difference between the uncorrected and the higher-order-corrected cross section.

Table 2 gives the correction factor f_c to the cross section due to high-order radiation effects in the photon beam for the present measurements used in our work. Instead of directly applying the correction function of Müller et al. (2015), we used an approximation by interpolating the values of f_c from Müller et al. (2015) listed in Table 2, and included values at 30 eV and 35 eV. From this approximation, we found that at 17.4 eV the total uncertainty is 33% and, at 19.64 eV the total uncertainty is already below 20%. Hence for the present experiment we quote a total error of 33% below 19.64 eV and 20% for higher energies in the spectrum.

3   THEORY

3.1   Atomic Structure

The GRASP code (Dyall et al. 1989; Parpia et al. 2006; Grant 2007) was used to generate the target wave functions employed in our collisions work. All orbitals were physical up to $n=3$, $4s$ and $4p$. We began by doing an extended averaged level (EAL) calculation for the $n = 3$ orbitals . All EAL calculations were performed on the lowest 24 fine-structure levels of the residual Zn III ion, in order to generate target wavefunctions for our photoionization studies. In our work we retained all the 355 - levels originating from one and two-electron promotions from the n=3 levels into the orbital space of this ion. All 355 levels from the sixteen configurations were included in the DARC close-coupling calculation, namely: $3s^2 3p^6 3d^{10}$, $3s^2 3p^6 3d^9 4s$, $3s^2 3p^6 3d^9 4p$, $3s^2 3p^5 3d^{10} 4s$, $3s^2 3p^5 3d^{10} 4p$, $3s 3p^6 3d^{10} 4s$, $3s 3p^6 3d^{10} 4p$, $3s^2 3p^6 3d^8 4s^2$, $3s^2 3p^6 3d^8 4p^2$, $3s^2 3p^6 3d^8 4s 4p$, $3s^2 3p^4 3d^{10} 4s^2$, $3s^2 3p^4 3d^{10} 4p^2$, $3s^2 3p^4 3d^{10} 4s 4p$, $3p^6 3d^{10} 4s^2$, $3p^6 3d^{10} 4p^2$ and $3p^6 3d^{10} 4s 4p$.

Table 3 gives a sample of the theoretical energy levels from the 355-level GRASP calculations for the lowest 17 levels of the residual Zn^{2+} ion, compared to the values available from the NIST tabulations (Kramida et al. 2016). The average percentage difference of our theoretical energy levels compared with the NIST values is approximately 12%. For the $3d^{10}$ $^1S_0 \rightarrow 3d^9 4p$ $^3P_1^o$ transition we obtained a value of 4.0×10^{-3} for the oscillator strength (f-value). This is to be compared with the f-value of 5.0×10^{-3}, for the same transition from the MCDF work of Yu et al. (2007). From our GRASP calculations, we obtained values of 1.3 ns and 1.8 ns for the radiative lifetimes for the 1581 Å and 1673 Å lines, respectively, the $3d^9 4p$ $^3F_4^o \rightarrow 3d^9 4s$ $^3D_3$ and $3d^9 4p$ $^3P_2^o \rightarrow 3d^9 4s$ $^3D_3$ transitions in Zn III. Our values are in respectable agreement with the experimental results of 1.1 ± 0.3 ns and 1.2 ± 0.3 ns from the previous work of Andersen et al. (1997).

Photoionization cross sections were then performed on the Zn II ion for the $3d^{10} 4s$ $^2S_{1/2}$ ground state and the $3d^9 4s^2$ $^2D_{3/2,5/2}$ metastable levels using the DARC codes, with these Zn III residual ion target wavefunctions.

3.2   Photoionization calculations

For comparison with high-resolution measurements made at the ALS, state-of-the-art theoretical methods with highly correlated wavefunctions that include relativistic effects are used. The scattering calculations were performed for photoionization cross sections using the above large-scale configuration interaction (CI) target wavefunctions as input to the parallel DARC suite of R-matrix codes.

The General Relativistic Atomic Structure Package (GRASP) (Dyall et al. 1989; Grant 2007) formulates and diagonalises a Dirac-Coulomb Hamiltonian (Grant 2007) to produce the relativistic orbitals for input to the Dirac Atomic R-matrix Code (DARC) (Chang 1975; Norrington & Grant 1981; Grant 2007; Burke 2011) to obtain the photoionization (PI) cross sections. These DARC codes are currently running efficiently on a variety of world-wide parallel High Performance Computer (HPC) architectures (Ballance 2016; McLaughlin & Ballance 2015; McLaughlin et al. 2015, 2016, 2017).

Table 3. Zn^{2+} energy levels in Rydbergs (Ry) from the large-scale GRASP calculations compared with the available tabulations from the NIST database (Kramida et al. 2016). A sample of the lowest 17 levels for the residual Zn^{2+} ion from the 355-level GRASP calculations are shown compared to experiment. The percentage difference $\Delta(\%)$ of individual energy levels is given for completeness.

Level	STATE	TERM	NIST (Ry)	GRASP (Ry)	$\Delta(\%)^a$
1	$3d^{10}$	$^1S_0$	0.000000	0.000000	0.0
2	$3d^94s$	$^3D_3$	0.711666	0.820402	15.3
3	$3d^94s$	$^3D_2$	0.722394	0.834832	15.6
4	$3d^94s$	$^3D_1$	0.736761	0.851328	15.6
5	$3d^94s$	$^1D_2$	0.760911	0.893474	17.4
6	$3d^94p$	$^3P^o_2$	1.256331	1.361426	8.4
7	$3d^94p$	$^3P^o_1$	1.276421	1.385355	8.5
8	$3d^94p$	$^3P^o_0$	1.288463	1.399012	8.6
9	$3d^94p$	$^3F^o_3$	1.281741	1.410420	10.0
10	$3d^94p$	$^3F^o_4$	1.287866	1.411489	9.6
11	$3d^94p$	$^3F^o_2$	1.298403	1.427982	10.0
12	$3d^94p$	$^1F^o_3$	1.316792	1.457057	10.7
13	$3d^94p$	$^1D^o_2$	1.323560	1.468436	10.9
14	$3d^94p$	$^3D^o_3$	1.330146	1.472693	10.7
15	$3d^94p$	$^3D^o_1$	1.344768	1.491643	11.0
16	$3d^94p$	$^3D^o_2$	1.347960	1.496767	11.0
17	$3d^94p$	$^1P^o_1$	1.344106	1.527372	13.6

^{a}Average $\Delta(\%)$ of the energy levels with experiment is $\approx 12\%$.

Fifteen continuum orbitals were used in our scattering calculations. A boundary radius of 9.61 a_0 was necessary to accommodate the diffuse $n = 4$ bound state orbitals of the residual Zn III ion. To fully resolve the resonance features present in the spectrum, an energy grid of 2.5×10^{-7} $\mathcal{Z}^2$ Ry (13.6 μeV), where $\mathcal{Z} = 2$, was utilized in our collision work.

Photoionization cross section calculations with this 355-level model were then performed with this fine energy mesh for the $3d^{10}4s$ $^2S_{1/2}$ ground state and the $3d^94s^2$ $^2D_{5/2,3/2}$ metastable levels of this ion, over the photon energy range similar to experimental studies. This insured that all the fine resonance features were fully resolved in the respective PI cross sections.

For the $^2S_{1/2}$ level we require the bound-free dipole matrices, $J^\pi = 1/2^e$, $\rightarrow J'^{\pi'} = 1/2^o$ and $3/2^o$. In the case of the $^2D_{5/2,3/2}$ metastable levels we required the $J^\pi = 3/2^e$, $\rightarrow J'^{\pi'} = 1/2^o$, $3/2^o$, $5/2^o$ and the $J^\pi = 5/2^e$, $\rightarrow J'^{\pi'} = 3/2^o$, $5/2^o$, $7/2^o$ bound-free dipole matrices. The jj-coupled Hamiltonian diagonal matrices were adjusted so that the theoretical term energies matched the recommended experimental values of the NIST tabulations (Kramida et al. 2016). We note that this energy adjustment ensures better positioning of resonances relative to all thresholds included in the present calculations.

3.3 Resonances

The energy levels available from the NIST tabulations (Kramida et al. 2016) were used as a helpful guide for the present assignments. The resonance series identification can be made from Rydberg's formula (Rydberg 1890, 1893, 1894; Eisberg & Resnik 1985) :

$$\epsilon_n = \epsilon_\infty - \frac{\mathcal{Z}^2}{\nu^2} \tag{3}$$

where in Rydbergs ϵ_n is the transition energy, ϵ_∞ is the ionization potential of the excited electron to the corresponding final state ($n = \infty$), i.e. the resonance series limit with n being the principal quantum number. The relationship between the principal quantum number n, the effective quantum number ν, and the quantum defect μ for an ion of effective charge $\mathcal{Z}$ is given by $\nu = n$ - μ (Shore 1967; Seaton 1983). Converting all quantities to eV, we can represent the Rydberg series as

$$E_n = E_\infty - \frac{\mathcal{Z}^2 \mathcal{R}}{(n - \mu)^2}. \tag{4}$$

Here, E_n is the resonance energy, E_∞ the resonance series limit, $\mathcal{Z}$ is the charge of the core (in this case $\mathcal{Z} = 2$), μ is the quantum defect ($\mu_{ns} > \mu_{np} > \mu_{nd} > \mu_{nf}, \ldots$), being zero for a pure hydrogenic state. For a hydrogenic system this can be written as

$$E_n^H = E_\infty - \frac{\mathcal{Z}^2 \mathcal{R}}{n^2}, \tag{5}$$

where the Rydberg constant $\mathcal{R}$ is $R_\infty = 13.605698$ eV.

The multi-channel R-matrix eigenphase derivative (QB) technique, which is applicable to atomic and molecular complexes, as developed by Berrington and co-workers (Quigley & Berrington 1996; Quigley et al. 1998; Ballance et al. 1999) was used to locate and determine the resonance positions. The resonance width Γ may also be determined from the inverse of the energy derivative of the eigenphase sum δ at the resonance energy E_r via

$$\Gamma = 2 \left[\frac{d\delta}{dE} \right]^{-1}_{E=E_r} = 2 \left[\delta' \right]^{-1}_{E=E_r}. \tag{6}$$

4 RESULTS AND DISSCUSSION

The ALS spectrum for the single photoionization of Zn^+ cross section measurements are illustrated in Fig. 1 (a) and (b), along with the absolute measurements and the results from the large-scale DARC PI cross section calculations. The ALS measurements were made in the photon energy range 17.5 eV – 90.0 eV with a photon energy resolution of 17 meV. In order to compare directly with experiment, the DARC results have been convoluted with a Gaussian having a profile width of 17 meV. PI calculations were performed for the ground state $3d^{10}4s$ $^2S_{1/2}$ and the $3d^94s^2$ $^2D_{3/2,5/2}$ metastable states. The absolute PI cross section measurements are shown in Fig. 1 (a) and (b) with open circles. Note, the correction factor f_c has not been applied to the ALS measurements. The DARC PI calculations are included in Fig. 1 (a) for 100% population of both the ground and metastable states. Fig. 1 (b) shows a comparison of the DARC PI cross section, convoluted using a Gaussian having
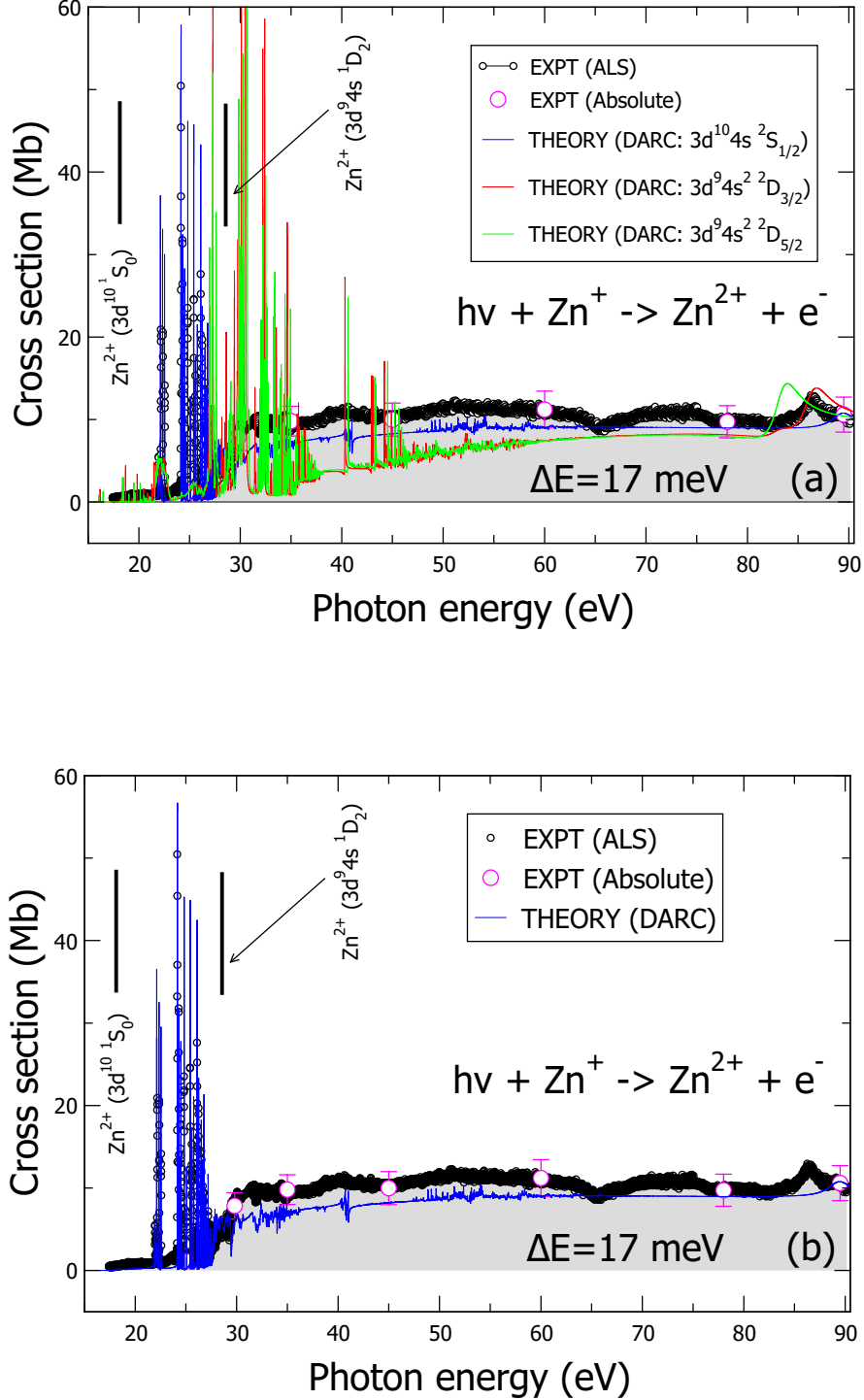
Figure 1. (Colour online) Single photoionization cross section of Zn^+ : ALS experimental data (open circles) and the 355-level Dirac *R*-matrix theoretical results. The ALS spectrum consists of Zn^{2+} ion yield spectra normalized to the absolute cross section measurements (magenta open circles). The thresholds for $Zn^{2+}(3d^{10}\ ^1S_0)$ at 17.964 eV and $Zn^{2+}(3d^94s\ ^1D_2)$ at 28.317 eV, respectively are indicated by vertical lines. The correction factor f_c has not been applied to the ALS data illustrated in the figures. (a) ALS measurements and the DARC PI calculations for the ground $(3d^{10}4s\ ^2S_{1/2})$ (blue line) and metastable $(3d^94s^2\ ^2D_{3/2}$ (red line) and $3d^94s^2\ ^2D_{5/2})$ (green line) contributions. (b) ALS measurements and the DARC PI calculations with an appropriate mixture of the ground and metastable states. See text for details
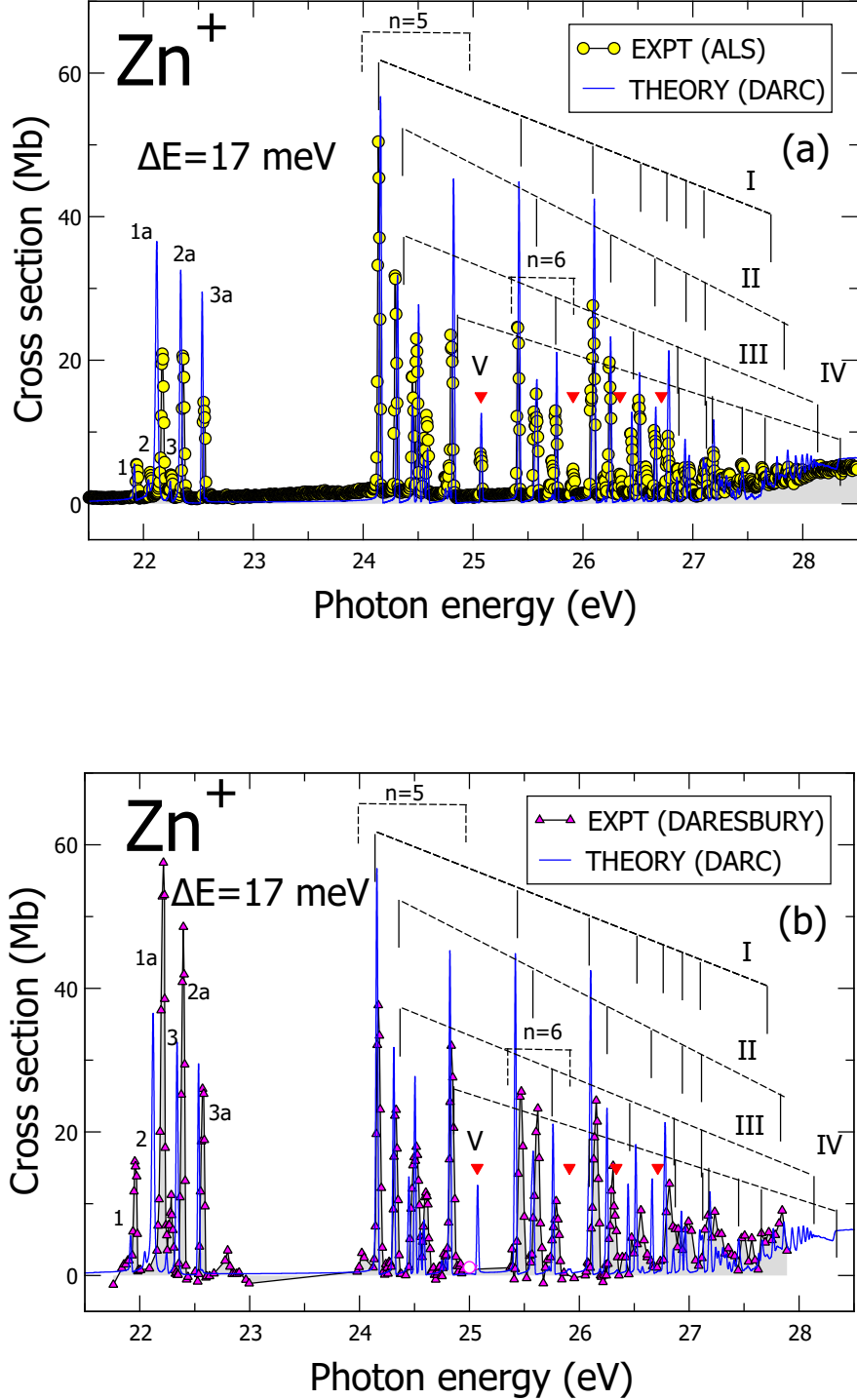
Figure 2. (Colour online) Single-photon, single photoionization cross section of Zn$^+$: Resonances features in the spectrum for 21.5 – 28.5 eV. (a) ALS measurements solid circles (yellow), resolution of 17 meV FWHM. (b) DARESBURY solid triangles (yellow) (Peart et al. 1987). In both panels the large-scale DARC calculations solid line (blue) are convoluted with a Gaussian, having a profile of 17 meV FWHM, with an appropriate admixture of ground and metastable states, see text for details. Vertical lines indicate the resonant energies of Table 4. The final vertical lines to the right of each group correspond to the limit of the series. Gaussian fits to the peak centres are tabulated in Tables 4 and 5. The grouped lines of the Rydberg series and vertical lines from panel (a) for those resonances that can be paired with a peak in the data by Peart et al. (1987). Open circle (magenta) is the ALS absolute cross section at 25 eV.
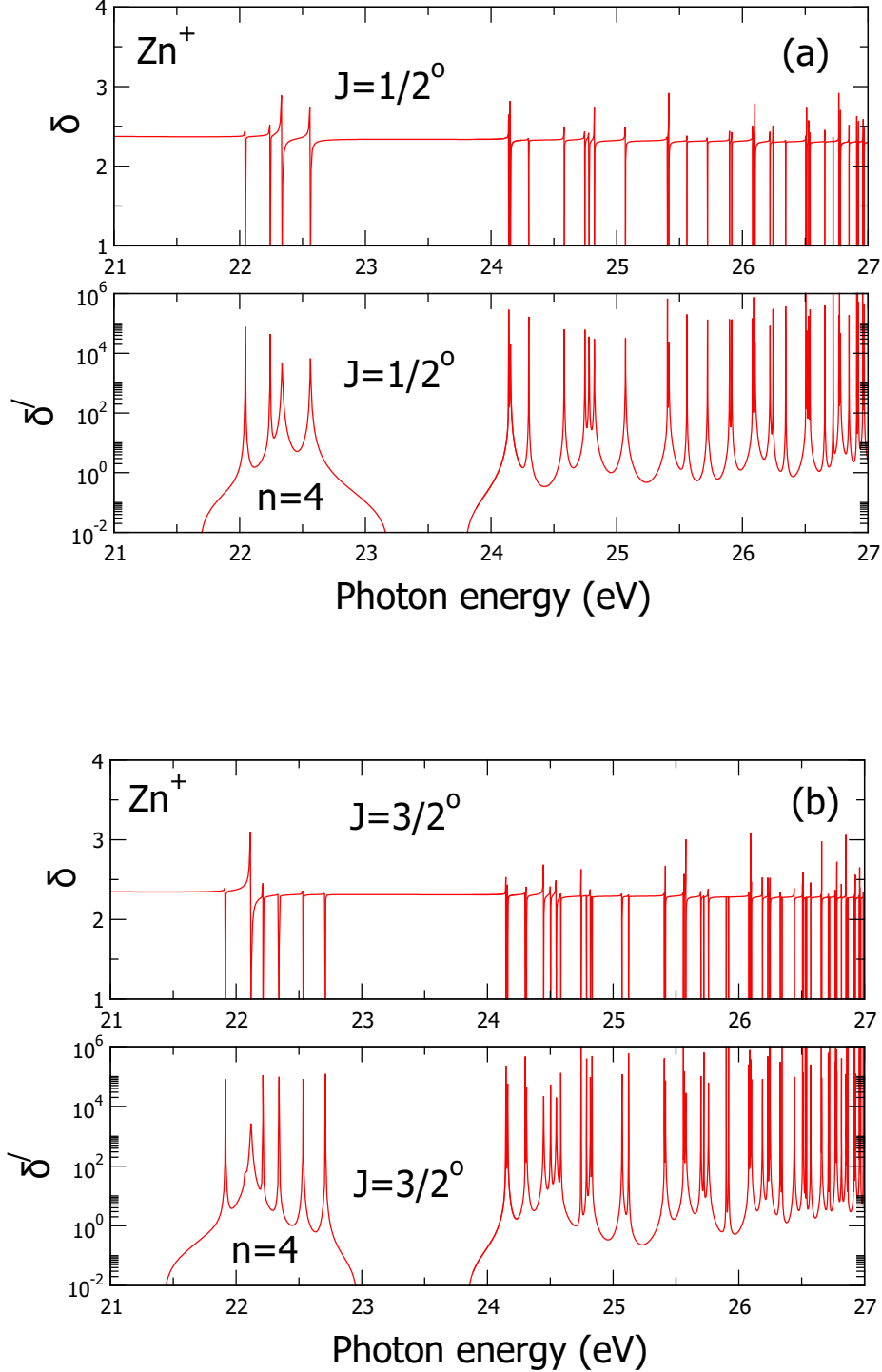
Figure 3. (Colour online) Eigenphase sum δ and its derivative δ' in the photon energy region 21 - 27 eV for (a) J=1/2 odd scattering symmetry, (b) J=3/2 odd scattering symmetry from the large - scale DARC PI calculations on the Zn II ion. Interloping and overlapping resonances series in the Zn II spectrum disrupt the regular Rydberg resonance series pattern. Tables 6 and 7 give assignments of resonances for each scattering symmetry.
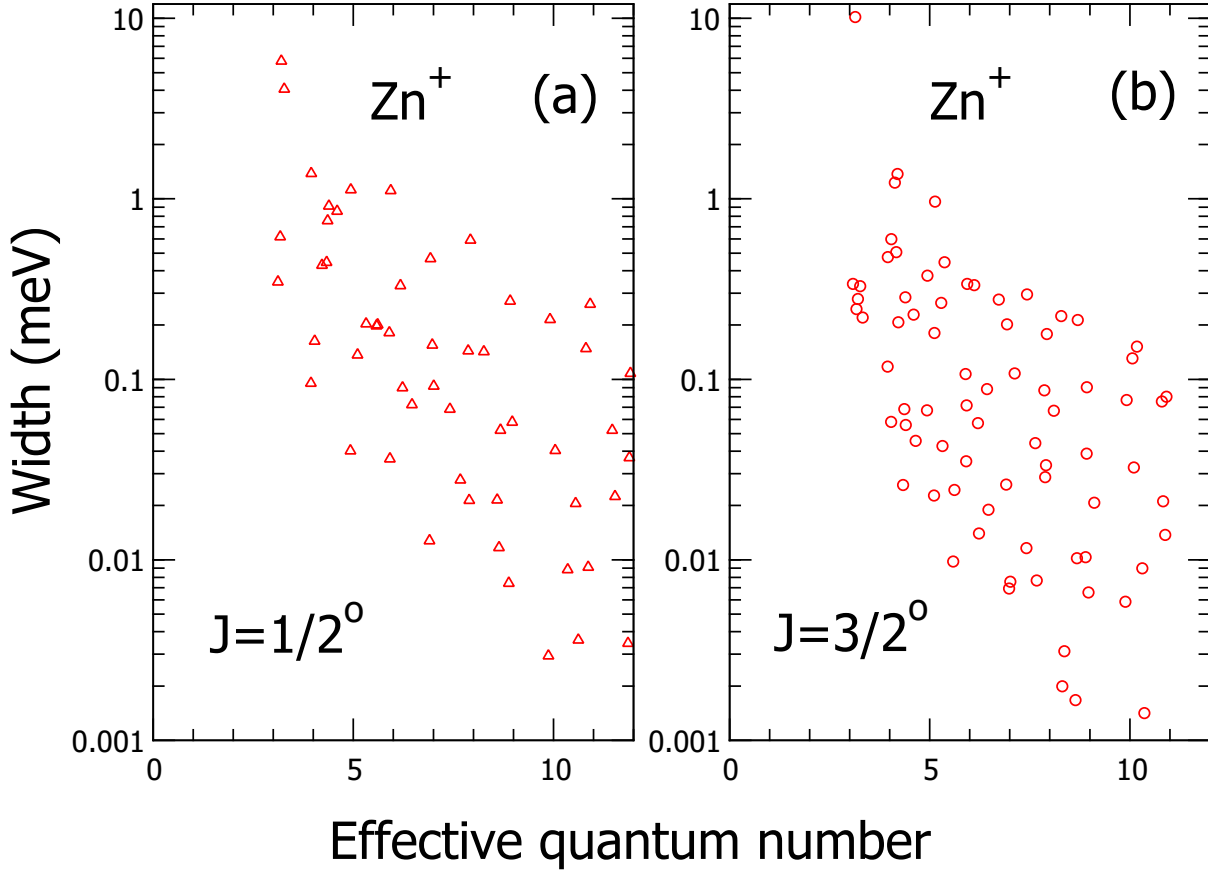
Figure 4. (Colour online) Resonance line widths Γ (meV) versus the effective quantum number ν for resonances series found in the Zn II ALS spectrum in the photon energy range 21 – 27 eV. (a) J=1/2 odd symmetry, (b) J=3/2 odd symmetry. The theoretical values were obtained using the eigenphase derivative method (Quigley & Berrington 1996; Quigley et al. 1998; Ballance et al. 1999) from the large-scale DARC calculations on the Zn II ion. The resonanances line widths are 10 meV or much less and impossible to be extracted with the present limited photon resolution of 17 meV FWHM.

a profile of 17 meV and an appropriate weighted admixture of 98% ground and 2% of the statistical average of the metastable states, with the ALS measurements. Excellent agreement is obtained between theory and experiment over the energy region investigated.

A restricted region of the spectrum, for the photon energy range 21.5 – 28.5 eV, is displayed in Fig. 2 (a) and (b). Fig. 2 (a) shows the present ALS spectrum recorded at 17 meV FWHW compared to the DARC calculations. In Fig. 2 (b) the previous Zn II digitized spectra obtained at the Daresbury radiation facility (Peart et al. 1987) are illustrated for the same energy region with a similar comparison made with the DARC calculations. In Figs. 2 (a) and (b), numerous sharp peak structures are seen in the Zn II spectrum over this energy region. The peaks in the spectrum can be assigned to well-defined Rydberg series originating from the ground state, namely, $Zn^+(3d^{10}4s\ {}^2S_{1/2})$ resonances, converging to the triplet state $3d^94s\ {}^3D_{3,2,1}$ thresholds (i.e. se-

ries I, II and III in panel (a) of Fig. 2), and to the singlet state threshold $3d^94s\ {}^1D_2$ (series IV) of the Zn^{2+} ion.

Series identification was guided by fitting equation (4) to a particular set of peak positions that corresponded to a well-defined series. The Rydberg series limits E_∞ were determined by fitting the series with equation (4), which agreed with results from the tabulations in the NIST database (Kramida et al. 2016), to three significant figures. Due to several overlapping peaks, values for the resonance energies were derived from Gaussian fits to the peaks to obtain more precise values for the peak centroids. These centroids are tabulated in Table 4, together with the averaged quantum defects μ_f and the corresponding series limits for the identified Rydberg resonance series.

In the resonant region of the spectrum 24 - 28 eV, it is seen that there are many interloping and overlapping resonances present. For some of the peaks, their resonance en-

ergies in Table 4 are given in parenthesis (or brackets) in order to indicate that they are estimates.

A resonance series with $n \geq 6$, labeled as series V in panel (a) of Fig. 2, (having small strengths), with the same series energy limit E_∞=27.647 eV of series I can be identified in the experimental spectrum. Excitation energies were calculated using the Cowan code (Cowan 1981; Mann 1983; Clark et al. 1991). To compare them with the measured resonance energies E_n (see Fig. 3), a linear fit was used where

$$E_n = m\ E_{\mathrm{Cowan}} + b \qquad (7)$$

with m and b constants (Müller et al. 2014). This function fitted the measured resonance energies very well for the excited state E_{Cowan} resonance energies.

Below 23 eV, a group of well-resolved resonances is observed, as indicated in panel (a) of Fig. 2. Higher-order radiation in the photon beam appears in the low energy interval of the first grating of the photon beamline, which may result in excitation of the Zn^+ energy levels accessible at higher photon energies. If this is the case, one would expect resonances to also appear at two or three times their photon energies. Since no such peaks were observed (see Fig.1 (a) and (b)) at the corresponding higher photon energies, one may conclude that higher-order photons are not the source of this particular set of resonances.

In panel (b) of Fig. 2 the earlier findings of Peart et al. (1987) are illustrated along with the DARC results. In this figure, as a guide, we have retained some of the grouping lines, labels, and a single absolute cross section data point from panel (a) of Fig. 2. The peaks reported by Peart et al. (1987) appear shifted toward higher energies, or shorter wavelengths, compared to the present ALS measurements and the DARC calculations. Differences are seen ranging from about 20 meV (in the lower energy regime), to 60 meV (in the higher energy regime) with their experiment. These differences we attribute to the energy calibration uncertainties reported by Lyon et al. (1986) of 30 meV to 77 meV, in the respective energy regimes. We note also that the DARC peak energies favour the ALS measurements as can be seen from Fig. 2 (a), (b) and the results tabulated in Table 5.

The peaks in the Zn II spectrum were identified from a theoretical analysis of the eigenphase sum δ and its derivative δ' for the J=1/2 and J=3/2 odd scattering symmetries obtained from the large-scale DARC calculations. The results are presented in Figs. 3 (a) and (b). We find that the peaks below 23 eV originate from photoionization of the ground state term and attribute them to excited resonance states $[3d^9 4s\ (^{1,3}\mathrm{D}_{3,2,1})\ 4p]_{1/2,3/2}$ converging to different Zn^{2+} core states. These are labeled, 1a – 3a and 1 – 3 in the experimental spectrum. The remaining peaks we can assign to well-defined Rydberg resonance series. We note that the $3d^9 4s\ (^3\mathrm{D}_3)\ 5p$ resonance, identified with series I, located at 24.141 eV, is the strongest in the spectrum.

An important feature of the spectrum of Fig.1 (a) and (b) is the small non-zero cross section below the ionization threshold (marked by vertical line). This shift is probably due to the presence of higher-order radiation in the photon beam which causes a contribution from the non-resonant cross section or from metastable contamination of the ion beam.

To determine the metastable contaminant in the ion beam, large-scale DARC PI calculations were performed for the $3d^9 4s^2\ ^2\mathrm{D}_{3/2,5/2}$ initial metastable states. From these DARC PI cross section calculations we determined that the metastable contamination of the ion beam was 2% by using a statistical average of the metastable theoretical cross sections compared to the ALS measurements at 17.5 eV. Hence we conclude that the resonance features in the spectrum originate from the ground state. Fig. 1 (a) shows the ALS measurements and the DARC PI calculations for the ground and metastable states, where 100% population of the ground and metastable states are assumed. In Fig. 1 (b), the DARC PI calculations have been appropriately weighted, 98% ground state and 2% of the statistical average of the metastable states. As can be seen from the results presented in Fig. 1 (a) and (b) there is excellent agreement between experiment and theory.

We note that in some cases, the populations of excited states in the ion beams have been estimated to be relatively low (Müller et al. 2014). For example, in a similar ion source, for C-like ions, using the MCDF method, the population of the $^5\mathrm{S}_2$ level was estimated to be $2 - 3\%$ (Bizau, J.-M. et al. 2005). In the present work by performing PI calculations for the metastable states indicated above we find their contribution is small, around 2%.

The prominent Rydberg resonance series are identified as $\mathrm{Zn}^+(3d^9 4s\ np)$ excitations, as indicated by the series labeled I, II, III and IV in panel (a) of Fig. 2.. Resonance energies E_n of each Rydberg resonance series found in the ALS spectrum are tabulated in Table 4 along with the averaged quantum defect μ_f for each series. A $\mathrm{Zn}^+(3d^9 4s\ np)$, $n \geq 6$, Rydberg resonance series, as indicated by the downward pointing solid triangles (red), see Figs. 2 (a) and (b), was also identified in the spectrum. The widths of many of these resonances found in the spectrum, as illustrated in Fig. 4 (a) and (b), are 10 meV or less making it impossible to extract values with the present limited experimental resolution of 17 meV. The quantum defects μ_n as a function of the principal quantum number n, for the dominant series are illustrated for the five series, I, II . . . , V, in Fig. 5.

An additional check on the theoretical data was carried out by comparing the integrated continuum oscillator strength f with experiment. The integrated continuum oscillator strength f of the experimental spectra was calculated over the energy grid $[E_1, E_2]$, where E_1 is the minimum experimental energy and E_2 is the maximum experimental energy measured, (respectively 17.409 eV and 91.142 eV), using (Shore 1967; Fano & Cooper 1968; Berkowitz 1979),

$$
\begin{aligned}
f &= 9.1075 \times 10^{-3} \int_{E_1}^{E_2} \sigma(h\nu) dh\nu \\
&= 9.1075 \times 10^{-3}\ \overline{\sigma}_{\mathrm{PI}}
\end{aligned}
$$

where

$$\overline{\sigma}_{\mathrm{PI}} = \int_{E_1}^{E_2} \sigma(h\nu) dh\nu \qquad (8)$$

is the resonance strength. Evaluating the continuum oscillator strength f for the ALS cross section measurements yielded a value of 5.743 ± 1.150, assuming an error of 20%. A similar procedure for the theoretical Dirac R-matrix cross sections gave a value of 4.966 for 98% of the

Table 4. Resonance energies E_n of the identified Rydberg series I, II, III, IV and V (from the present experimental ALS data) converging to the $3d^94s$ $^3D_{3,2,1}$ triplet and the $3d^94s$ $^1D_2$ singlet states originating from the Zn^+ ground state. Some energies, in brackets, have the same superscript to indicate that they superimpose. In some cases, multi-peak Gaussian fits were used to try to improve assignments when possible. Roman number labels correspond to those of Fig. 2. The average value of the quantum defect μ_f for the Rydberg series corresponds to the value of μ derived from direct fitting to equation (4). Values in parenthesis or brackets are estimates from the fits.

|	Autoionizing Zn II Rydberg resonance series energies				
	I	II	III	IV	V
	$(3d^94s)^3D_3$ np	$(3d^94s)^3D_2$ np	$(3d^94s)^3D_1$ np	$(3d^94s)^1D_2$ np	$(3d^94s)^3D_3$ np
n	E_n(eV)	E_n(eV)	E_n(eV)	E_n(eV)	E_n(eV)
5	24.141	24.294	24.488	24.804	–
6	25.408	25.569	25.752	[26.069][1]	25.071
7	[26.093][1]	26.243	26.439	[26.773][2]	25.910
8	26.512	26.656	26.858	[27.184][4]	(26.340)
9	[26.773][2]	26.926	[27.116][3]	27.450	(26.714)
10	26.966	[27.104][3]	–	27.632	–
11	[27.087][3]	–	–	27.767	–
12	[27.184][4]	–	–	27.863	–
13	(27.253)	–	–	27.939	–
14	–	–	–	27.994	–
15	–	–	–	28.041	–
⋮					
Limit	27.647	27.793	27.989	28.317	27.647
μ_f	1.11 ± 0.2	1.08 ± 0.2	1.07 ± 0.2	1.05 ± 0.2	1.43 ± 0.3

Table 5. Resonance energies (E_n) and strengths ($\overline{\sigma}_{PI}$) from the ALS data only for those peaks resolved in the DARESBURY data of Peart et al. (1987) where a comparison is possible. The resonance strengths $\overline{\sigma}_{PI}$ derived from the present ALS data have been multiplied by f_c. Resonance strengths and positions were determined from the large-scale 355-level DARC calculations, assuming 100% of the ground state. The resonance positions for the DARC values were estimated by fitting the peaks in the total cross sections to Fano profiles. Values in brackets shown (98% of the ground state) are corrected for metastable contamination in the ion beam, determined to be 2%, see text for details.

Resonance	ALS[a]		DARESBURY[b]		DARC[c]	
Label	E_n (eV)	$\overline{\sigma}_{PI}$ ($Mb\ eV$)	E_n (eV)	$\overline{\sigma}_{PI}$ ($Mb\ eV$)	E_n (eV)	$\overline{\sigma}_{PI}$ ($Mb\ eV$)
$n = 4$						
1 (J=3/2)	21.940	0.19 ± 0.05	21.958	0.55	21.919	0.19 (0.18)
1a (J=3/2)	22.173	0.87 ± 0.21	22.210	2.50	22.123	1.22 (1.20)
2a (J=1/2)	22.361	0.69 ± 0.20	22.393	1.70	22.340	0.72 (0.71)
3a (J=3/2)	22.552	0.42 ± 0.13	22.573	0.98	22.535	0.45 (0.44)
$n = 5$	24.141	1.52 ± 0.50	24.172	1.60	24.158	1.42 (1.39)
	24.294	0.99 ± 0.31	24.329	0.98	24.312	0.83 (0.81)
	24.488	0.64 ± 0.23	24.509	1.36	24.504	0.53 (0.52)
	24.804	0.84 ± 0.24	24.839	1.57	25.824	0.97 (0.95)
$n = 6$	25.408	0.77 ± 0.25	25.468	1.34	25.418	1.04 (1.02)
	25.569	0.75 ± 0.15	25.616	1.24	25.577	0.64 (0.63)
	25.752	0.35 ± 0.13	25.786	0.70	25.762	0.41 (0.40)
$n = 7$	(26.093)	(1.13 ± 0.28)	26.150	1.28	26.102	1.32 (1.29)
	26.243	0.62 ± 0.20	26.305	0.77	26.251	0.65 (0.84)

[a] ALS, present experiment.
[b] DARESBURY, previous experimental results (Peart et al. 1987).
[c] DARC, present theory, 355-level approximation.
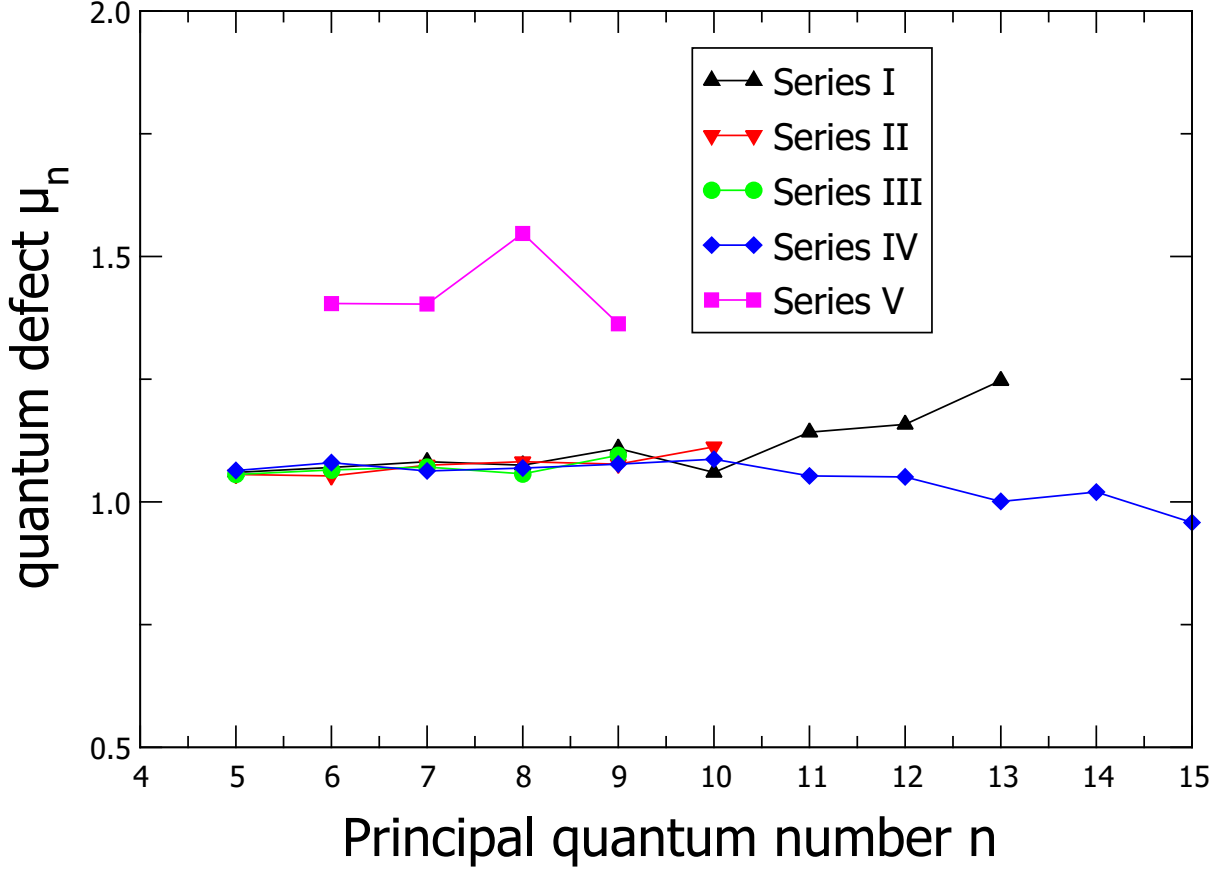
Figure 5. (Colour online) Quantum defect μ_n versus the principal quantum number n for the dominant resonances series found in the Zn II ALS measured spectrum for the photon energy range 24 – 28 eV. Table 4 gives details for resonance series labeled I, II, III, IV and V.

Table 6. Resonance energies E_n of the identified Rydberg series I, II, III, IV and V (from the large-scale DARC calculations), J=1/2 odd scattering symmetry, converging to the $3d^9 4s\ ^3D_{3,2,1}$ triplet and the $3d^9 4s\ ^1D_2$ singlet states originating from the Zn^+ ground state.

	Autoionizing Zn II Rydberg resonance series energies, J=1/2° symmetry				
	I	II	III	IV	V
	$(3d^9 4s)^3D_3\ np$	$(3d^9 4s)^3D_2\ np$	$(3d^9 4s)^3D_1\ np$	$(3d^9 4s)^1D_2\ np$	$(3d^9 4s)^3D_3\ np$
n	E_n(eV)	E_n(eV)	E_n(eV)	E_n(eV)	E_n(eV)
4	–	22.044	–	22.337	22.563
5	24.149	24.583	24.141	24.747	24.780
6	25.415	25.559	25.404	25.723	25.723
7	26.101	26.220	26.082	26.345	26.345
8	26.512	26.538	26.504	26.656	26.659
9	26.780	26.849	26.773	26.909	26.910
10	26.962	26.147	26.957	27.088	27.088
$\vdots$					
Limit	27.647	27.793	27.989	28.317	27.647

Table 7. Resonance energies E_n of the identified Rydberg series I, II, III, IV and V (from the large-scale DARC calculations), J=3/2 odd scattering symmetry, converging to the $3d^9 4s\ ^3D_{3,2,1}$ triplet and the $3d^9 4s\ ^1D_2$ singlet states originating from the Zn$^+$ ground state.

	Autoionizing Zn II Rydberg resonance series energies, J=3/2° symmetry				
	I $(3d^9 4s)^3D_3\ np$	II $(3d^9 4s)^3D_2\ np$	III $(3d^9 4s)^3D_1\ np$	IV $(3d^9 4s)^1D_2\ np$	V $(3d^9 4s)^3D_3\ np$
n	E_n(eV)	E_n(eV)	E_n(eV)	E_n(eV)	E_n(eV)
4	–	22.214	21.916	22.213	22.711
5	24.148	24.311	24.447	24.503	24.745
6	25.417	25.573	24.564	25.579	25.759
7	26.101	26.243	26.233	26.330	26.330
8	26.512	26.656	26.572	26.656	26.572
9	26.780	26.858	26.853	26.868	26.817
10	26.963	26.991	–	26.991	26.991
⋮					
Limit	27.647	27.793	27.989	28.317	27.647

$3d^{10}4s\ ^2S_{1/2}$ ground state and 2% of the statistical average of the $3d^9 4s^2\ ^2D_{3/2}$ and $3d^9 4s^2\ ^2D_{5/2}$ metastable states, in good agreement with experiment. We note that for an individual resonance strength $\overline{\sigma}_{PI}$, the energy grid $[E_1, E_2]$ is over only the energy span of the resonance. We have used this procedure to determine the resonance strengths from our work.

For the peaks that are well resolved, in the Peart et al. (1987) data, resonance strengths have been derived and are compared with values obtained from the ALS measurements and the DARC calculations. The results are tabulated in Table 5. In general, the resonance strengths of Peart et al. (1987) are much larger than the corresponding values determined from our work. It is seen that only two resonant peaks (with comparable values) are within the uncertainties of both measurements, i.e., the two first peaks of group n=5.

It is important to point out that Peart et al. (1987) used an electron bombardment ion source of zinc vapor to generate their Zn$^+$ ion beam. In a study of emission cross sections for electron-impact excitation of Zn$^+$, Rogers et al. (1982) used the same type of hot-filament ion source with vaporized zinc metal. They found a large background signal due to higher-lying metastable Zn$^+$ ions in their beam. Metastable contamination in the Zn$^+$ ion beam was lowered by reducing the ion-source anode voltage to 12 V. Peart et al. (1987) studied the effect on the population of electronic excitation in their ion source by changing the voltage of the anode of their ion source. In this type of ion source, the amount of electronic excitation can be controlled by changing the anode voltage, since at low pressures, this voltage corresponds to the electron impact kinetic energy. In studies of emission cross sections for electron impact excitation of Zn$^+$ ions, Rogers et al. (1982) showed a difference of less than 20% in the excitation cross section between the voltages that Peart et al. (1987) used in their comparison (13.4 V and 23.0 V).

This relatively small change in the electron-impact excitation cross section of Zn$^+$ for the two electron kinetic energies, combined with a substantial population of ground state Zn$^+$, implied that the ion beam was in almost the same internal energy at both anode voltages. This explains why they did not observe any measurable differences in their photoionization cross section as a function of the anode potential. Electron impact generates electronic excitation. A possible explanation for the disagreement in the resonance strengths is that the ion beam population of electronically excited states of Peart et al. (1987) were different than the population of excited states in the ion beam of the present ALS experiment.

5 CONCLUSIONS

Photoionization cross sections producing Zn^{2+} from Zn$^+$ ions were measured in the photon energy range of 17.5 eV – 90 eV with a photon energy resolution of 17 meV FWHM. All the sharp resonance features present in the spectrum (for the energy region 20 – 28 eV) have been analyzed and identified. These resonance features we attribute to Rydberg transitions originating from the ground state Zn$^+$ into excited autoionizing states of the Zn$^+$ ion that ionize to the different $3d^9 4s\ ^3D_{3,2,1}$ and $3d^9 4s\ ^1D_2$ threshold states of Zn^{2+}. We note that the DARC calculations, for resonance energies and peak heights, favour the present ALS measurements as opposed to the previous measurements from the Daresbury radiation facility (Peart et al. 1987).

The most prominent peak in the spectrum is observed at 24.141 eV in the ALS data, 24.172 eV in the Daresbury data (Peart et al. 1987) and 24.158 eV in the DARC calculations, a difference of 31 meV and 17 meV respectively, see Table 5. We attribute this peak to an excited Zn$^+[3d^9 4s(^3D_3)\ 5p]$ autoionizing resonant state, originating from photoexcitation of the $3d^{10}4s\ ^2S_{1/2}$ ground state and decaying back to the state $3d^9 4s\ (^3D_3)$ of Zn^{2+}. This autoionizing state is a member of the Rydberg resonance series I, see panel (a) of Fig. 2. We note that transitions from the electronically excited $3d^{10}4p\ ^2P^o_{1/2,3/2}$ levels are dipole allowed to the $3d^{10}4s\ ^2S_{1/2}$ ground state and will not be present in the spectrum.

The cross section below the ground state threshold at 17.964 eV does not go to zero, due to a small fraction of

excited metastable states present in the Zn^+ ion beam. In addition, contributions from higher-order radiation components may contaminate the photon beam. A comparison of the present results with the earlier measurements of Peart et al. (1987) reproduces all their resonant peaks but with much improved statistics. Discrepancies in the cross sections in the low-energy regime of the spectrum we attribute to the different populations of the excited and metastable states in the ion beams of both experiments.

Interpretation of the present data was made possible using photoionization cross section results determined from large-scale Dirac *R*-matrix calculations which allows for the inclusion of the interaction between closed and open channels. We traced the contributions from different initial states in the ion beam and determined the metastable fraction present in the experiment to be small, in the region of 2%.

ACKNOWLEDGEMENTS

REFERENCES

Andersen T., Pedersen P., Biemont E., 1997, JQSRT, **17**, 389
Ballance C. P., 2016, DARC codes website URL, http://connorb.freeshell.org
Ballance C. P., Berrington K. A., McLaughlin B. M., 1999, Phys. Rev. A, **60**, R4217
Berkowitz J., 1979, Photoabsorption, Photoionization and Photoelectron Spectroscopy. Academic Press, New York, USA
Bizau, J.-M. et al., 2005, A&A, **439**, 387
Burke P. G., 2011, R-Matrix Theory of Atomic Collisions: Application to Atomic, Molecular and Optical Processes. Springer, New York, USA
Busso M., Gallino R., Wasserburg G. J., 1999, ARA&A, **37**, 239
Cardelli J. A., Federman S. R., Lambert D. L., Theodosiou C. E., 1993, ApJ, **416**, L41
Chang J. J., 1975, J. Phys. B: At. Mol. Opt. Phys., **8**, 2327
Chayer P., Vennes S., Dupuis J., Kruk J. W., 2005, ApJ, **630**, L169
Chen Y. Q., Nissen P. E., Zhao G., 2004, A&A, **425**, 697
Clark R. E. H., Abdallah Jr. J., Mann J., 1991, ApJ, **381**, 597
Covington A. M., et al., 2002, Phys. Rev. A, **66**, 062710
Cowan R. D., 1981, The Theory of Atomic Structure and Spectra. University of California Press, Berkeley, California, USA
Cowan J. J., Sneden C., 2006, Nature, **440**, 1151
Djeniže, S. Milosavljevic, V. Dimitrijevic, M. S. 2003, Eur. Phys. J. D, **27**, 209
Domke M., Schulz K., Remmers G., Kaindl G., Wintgen D., 1996, Phys. Rev. A, **53**, 1424
Dyall K. G., Johnson C. T., Grant I. P., Parpia F., Plummer E. P., 1989, Comput. Phys. Commun., **55**, 425
Eisberg R. E., Resnik R. M., 1985, Quantum Physics of Atoms, Molecules, Solids Nuclei and Particles, 2nd edn. Wiley, New York, USA
Esteves D. A., Bilodeau R. C., Sterling N. C., Phaneuf R. A., Kilcoyne A. L. D., Red E. C., Aguilar A., 2011, Phys. Rev. A, **84**, 013406
Esteves D. A., Bilodeau R. C., Phaneuf R. A., Kilcoyne A. L. D., Red E. C., Aguilar A., 2012, J. Phys. B: At. Mol. Opt. Phys., **45**, 115201
Fano U., Cooper J. W., 1968, Rev. Mod. Phys., **40**, 441
Frebel A., Simon J. D., Kirby E. N., 2014, ApJ, **786**, 74
Ganeev R. A., Suzuki M., Yoneya S., Strelkov V. V., Kuroda H., 2016, J. Phys. B: At. Mol. Opt. Phys., **49**, 055402
García-Rojas J., Madonna S., Luridiana V., Sterling N. C., Morisset C., Delgado-Inglada G., Toribio San Cipriano L., 2015, MNRAS, **452**, 2606
García-Rojas J., Peña M., Flores-Durán S., Hernández-Martínez L., 2016, A&A, **586**, A59
Grant I. P., 2007, Quantum Theory of Atoms and Molecules: Theory and Computation. Springer, New York, USA
Harrison H., Schoen R. I., Cairns R. B., Schubert K. E., 1969, J. Chem. Phys., **50**, 3930
Herwig F., 2005, ARA&A, **43**, 435
Hinkel N. R., Timmes F., Young P. A., Pagano M. D., Turnbull M. C., 2014, Astron. J., **148**, 54
Hollek J. K., Frebel A., Roederer I. U., Sneden C., Shetrone M., Beers T. C., Kang S., Thom C., 2011, ApJ, **742**, 54
Jose J., Iliadis C., 2011, Rep. Prog. Phys., **74**, 096901
Karakas A. I., van Raai M. A., Lugaro M., Sterling N. C., Dinerstein H. L., 2009, ApJ, **690**, 1130
King G. C., Tronc M., Read F. H., Bradford R. C., 1977, J. Phys. B: At. Mol. Phys., **10**, 2479
Kobayashi C., Nomoto K., 2009, ApJ, **707**, 1466
Kramida A. E., Ralchenko Y., Reader, J. and NIST ASD Team 2016, NIST Atomic Spectra Database (version 5.3), National Institute of Standards, Technology, Gaithersburg, MD, USA, http://physics.nist.gov/
Langanke K., Wiescher M., 2001, Rep. Prog. Phys., **64**, 1657
Lyon I. C., Peart B., West J. B., Dolder K., 1986, J. Phys. B: At. Mol. Phys., **19**, 4137
Lyon I. C., Peart B., Dolder K., West J. B., 1987, J. Phys. B: At. Mol. Phys., **20**, 1471
Macaluso D. A., Aguilar A., Kilcoyne A. L. D., Red E. C., Bilodeau R. C., Phaneuf R. A., Sterling N. C., McLaughlin B. M., 2015, Phys. Rev. A, **92**, 063424
Mann J. B., 1983, ADNDT, **29**, 407
McLaughlin B. M., Ballance C. P., 2012a, J. Phys. B: At. Mol. Opt. Phys., **45**, 085701
McLaughlin B. M., Ballance C. P., 2012b, J. Phys. B: At. Mol. Opt. Phys., **45**, 095202
McLaughlin B. M., Ballance C. P., 2015, in Resch M. M., Kovalenko Y., Fotch E., Bez W., Kobaysah H., eds, , Sustained Simulated Performance 2014. Springer, Berlin, Germany, pp 173–190
McLaughlin B. M., Ballance C. P., Pindzola M. S., Müller A., 2015, in Nagel W. E., Kröner D. H., Resch M. M., eds, ,

High Performance Computing in Science and Engineering'14. Springer, Berlin, Germany, pp 23–40

McLaughlin B. M., Ballance C. P., Pindzola M. S., Schippers S., Müller A., 2016, in Nagel W. E., Kröner D. H., Resch M. M., eds, , High Performance Computing in Science and Engineering'15. Springer, Berlin, Germany, pp 51–74

McLaughlin B. M., Ballance C. P., Pindzola M. S., Stancil P. C., Schippers S., Müller A., 2017, in Nagel W. E., Kröner D. H., Resch M. M., eds, , High Performance Computing in Science and Engineering'16. Springer, Berlin, Germany, pp 33–48

Mendenhall M. H., Henins A., Hudson L. T., Szabo C. I., Windover D., P Cline J. P., 2017, J. Phys. B: At. Mol. Opt. Phys., **50**, 115004

Mishenina T. V., Kovtyukh V. V., Soubiran C., Travaglio C., Busso M., 2002, A&A, **396**, 189

Müller M., Schmidt M., Zimmermann P., 1986, Eur. Phys. Letts., **2**, 359

Müller A., et al., 2014, J. Phys. B: At. Mol. Opt. Phys., **47**, 215202

Müller A., Schippers S., Hellhund J., Holste K., Kilcoyne A. L. D., Phaneuf R. A., Ballance C. P., McLaughlin B. M., 2015, J. Phys. B: At. Mol. Opt. Phys., **48**, 235203

Nissen P. E., Chen Y. Q., Asplund M., Pettini M., 2004, A&A, **415**, 993

Nissen P. E., Akerman C., Asplund M., Fabbian D., Kerber F., Keufl H. U., Pettini M., 2007, A&A, **469**, 319

Norrington P. H., Grant I. P., 1981, J. Phys. B: At. Mol. Phys., **14**, L261

Parpia F., Froese-Fisher C., Grant I. P., 2006, Comput. Phys. Commun., **94**, 249

Peart B., Stevenson J. G., Dolder K. T., 1973, J. Phys. B: At. Mol. Phys., **6**, 146

Peart B., Lyon I. C., Dolder K. I., 1987, J. Phys. B: At. Mol. Phys., **20**, 5403

Quigley L., Berrington K. A., 1996, J. Phys. B: At. Mol. Opt. Phys., **29**, 4529

Quigley L., Berrington K. A., Pelan J., 1998, Comput. Phys. Commun., **114**, 225

Roederer I. U., 2012, ApJ, **758**, 36

Roederer I. U., Sneden C., Thompson I. B., Preston G. W., Shectman S. A., 2010, ApJ, **711**, 573

Roederer I. U., Marino A. F., Sneden C., 2011, ApJ, **742**, 37

Roederer I. U., et al., 2014, ApJ, **791**, 32

Rogers W. T., Stefani G., Camilloni R., Dunn G. H., Mezanne A. Z., Henry R. J. W., 1982, Phys. Rev. A, **25**, 737

Rydberg J. R., 1890, Phil. Mag., **29**, 331

Rydberg J. R., 1893, Ann. Phys., **50**, 625

Rydberg J. R., 1894, Ann. Phys., **52**, 119

Seaton M. J., 1983, Rep. Prog. Phys., **46**, 167

Sharpee B., Zhang Y., Williams R., Pellegrini E., Cavagnolo K., Baldwin J. A., Phillips M., Liu X.-W., 2007, ApJ, **659**, 1265

Shore B. W., 1967, Rev. Mod. Phys., **39**, 439

Smith V. V., Lambert D. L., 2015, ApJS, **72**, 387

Sneden C., Gratton R. G., Crocker D. A., 1991, A&A, **246**, 354

Stener M., Decleva P., 1997, J. Phys. B: At. Mol. Opt. Phys., **30**, 4481

Sterling N. C., Dinerstein H. L., 2008, ApJS, **174**, 154

Sterling N. C., Stancil P. C., 2011, A&A, **535**, A117

Sterling N. C., Witthoeft M. C., 2011, A&A, **529**, A147

Sterling N. C., Dinerstein H. L., Kallman T. R., 2007, ApJS, **169**, 37

Sterling N. C., et al., 2009, Publ. Astron. Soc. Aust., **26**, 339

Sterling N. C., Esteves D. A., Bilodeau R. C., Kilcoyne A. L. D., Red E. C., Phaneuf R. A., Aguilar A., 2011a, J. Phys. B: At. Mol. Opt. Phys., **44**, 025701

Sterling N. C., et al., 2011b, Can. J. Phys., **89**, 379

Sterling N. C., Porter R. L., Dinerstein H. L., 2015, ApJS, **218**, 25

Sterling N. C., Dinerstein H. L., Kaplan K. F., Bautista M. A.,

2016, ApJ, **819**, L9

Travaglio C., Gallino R., Arnone E., Cowan J. J., Jordan F., Sneden C., 2004, ApJ, **60**, 186

Tumlinson J., 2006, ApJ, **641**, 1

Wallerstein G., et al., 1997, Rev. Mod. Phys., **69**, 995

Yu Y. G., Li J. G., Dong C. Z., Ding X. B., Fritzsche S., Fricke B., 2007, Eur. Phys. J. D, **44**, 51

This paper has been typeset from a TeX/LaTeX file prepared by the author.